ACS APPLIED MATERIALS & INTERFACES

www.acsami.org

Research Article

NiN-Passivated NiO Hole-Transport Layer Improves Halide Perovskite-Based Solar Cell

Anat Itzhak,[‖] Xu He,[‖] Adi Kama, Sujit Kumar, Michal Ejgenberg, Antoine Kahn,* and David Cahen*

Cite This: *ACS Appl. Mater. Interfaces* 2022, 14, 47587−47594

Read Online

ACCESS | Metrics & More | Article Recommendations | Supporting Information

ABSTRACT: The interfaces between inorganic selective contacts and halide perovskites (HaPs) are possibly the greatest challenge for making stable and reproducible solar cells with these materials. NiO_x, an attractive hole-transport layer as it fits the electronic structure of HaPs, is highly stable and can be produced at a low cost. Furthermore, NiO_x can be fabricated via scalable and controlled physical deposition methods such as RF sputtering to facilitate the quest for scalable, solvent-free, vacuum-deposited HaP-based solar cells (PSCs). However, the interface between NiO_x and HaPs is still not well-controlled, which leads at times to a lack of stability and V_{oc} losses. Here, we use RF sputtering to fabricate NiO_x and then cover it with a Ni_yN layer without breaking vacuum. The Ni_yN layer protects NiO_x doubly during PSC production. Firstly, the Ni_yN layer protects NiO_x from Ni^{3+} species being reduced to Ni^{2+} by Ar plasma, thus maintaining NiO_x conductivity. Secondly, it passivates the interface between NiO_x and the HaPs, retaining PSC stability over time. This double effect improves PSC efficiency from an average of 16.5% with a 17.4% record cell to a 19% average with a 19.8% record cell and increases the device stability.

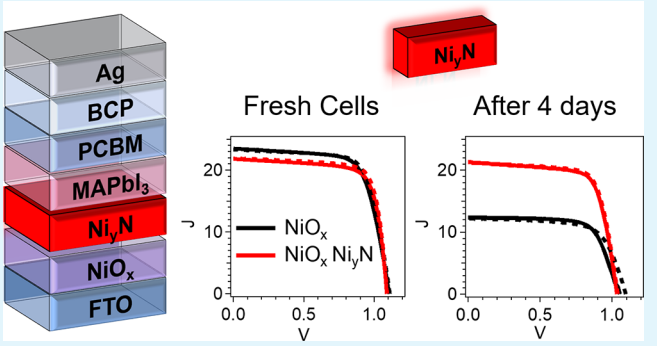

KEYWORDS: *halide perovskites, solar cells, nickel oxide, nickel nitride, passivation, interface*

INTRODUCTION

Halide perovskite solar cells (PSCs) have been extensively researched since 2009, and their power conversion efficiency (PCE) has improved toward their Shockley−Queisser limit. One of the main factors for the high PCE in PSCs composed of polycrystalline thin films is the intrinsically low defect concentration in the bulk of halide perovskites (HaPs).[1−3] However, PSCs are not constructed from HaPs alone, and defect states at interfaces between HaP films and adjacent layers adversely affect the conversion efficiency, long-term stability, and reproducibility of PSCs.[4,5]

Nickel oxide (NiO_x) is a sturdy and efficient hole-transport material (HTM), which has been reported to improve the stability of PSCs over that achieved with organic HTMs.[6−9] Radio-frequency (RF) sputtering is a scalable fabrication method for metal oxides with a highly controlled oxygen partial pressure. Wang et al. have shown that sputtered NiO_x at low temperatures has controlled transparency and conductivity that affect the efficiency of the PSC.[10] Moreover, sputtered NiO_x is preferred over wet-chemically processed NiO_x because it leaves no residues of solvents or precursors that can damage the stability and efficiency of the final device.[11] However, sputtered NiO_x hole-transport layers (HTLs) with no further treatment have parasitic resistance that leads to PSCs with moderate fill factors (FFs) and efficiencies.[12−14]

One of the challenges of using NiO_x as HTM is its nonstoichiometric composition; Ni^{2+} readily oxidizes into Ni^{3+}. Then, charge balance leads to a Ni-poor material, NiO_x with, i.e., $x < 1$, which is a p-type semiconductor due to Ni vacancies. Excess oxygen in more conductive NiO_x leads to more Ni^{3+} species.[15] On the one hand, the Ni^{3+} cations are essential as dopants to improve NiO_x conductivity.[16,17] On the other hand, the same Ni^{3+} cation is highly reactive and leads to degradation of the adjacent HaP layer in the solar device.[14]

Earlier attempts to passivate the NiO_x/HaP interface have improved PSC efficiency and stability.[18−20] Most passivation techniques have so far included deposition of a buffer layer through spin coating[21,22] or introducing additives into the HaP solution.[23] These passivation approaches are not suited for the fabrication of larger area perovskite devices that would inevitably need solvent-less methods, for both active layer deposition and interface modification.[24,25]

Received: July 1, 2022
Accepted: September 28, 2022
Published: October 13, 2022

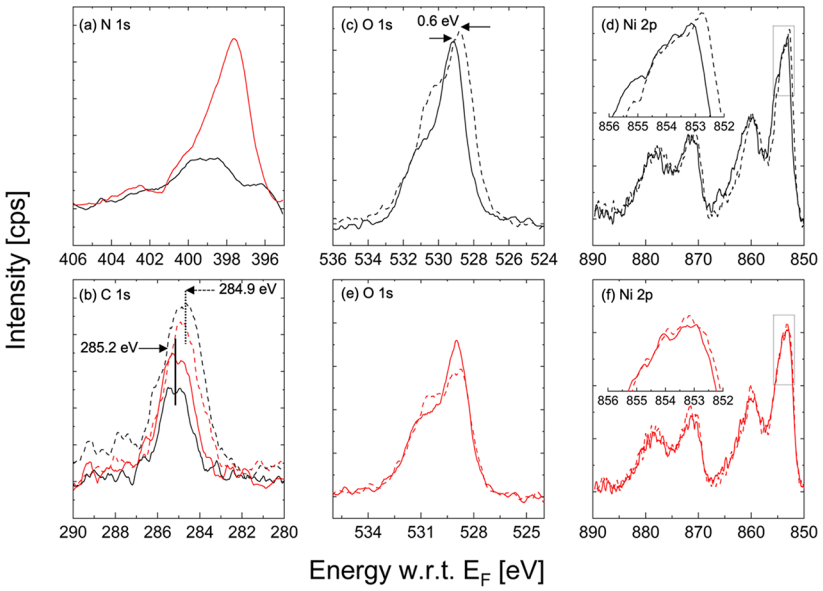

Figure 1. Narrow-range XPS plots of the (a) N 1s peak of a reference NiO_x (black) and Ni_yN-modified NiO_x (red), (b) C 1s peak of a reference NiO_x (black) and Ni_yN-modified NiO_x (red) before (dashed) and after (solid) Ar^+ etching, (c) O 1s and (d) Ni 2p peaks of a reference NiO_x before (dashed) and after (solid) Ar^+ etching, and (e) O 1s and (f) Ni 2p peaks of a Ni_yN-modified NiO_x before (dashed) and after (solid) Ar^+ etching.

In this work, we use RF magnetron sputtering for an alternative in-situ route to passivate the HaP/NiO_x interface. The approach is well-suited for upscaling PSC throughput via all vacuum-processed device fabrication techniques. We deposit nickel nitride (Ni_yN), a very small bandgap semiconductor, as an ultra-thin ~2 nm layer on NiO_x, essentially an in-situ modification of the NiO_x surface without breaking vacuum. This Ni_yN interlayer becomes a buffer between the oxide and the HaP film. We then investigate its effects on PSC performance and stability.

We find that Ni_yN protects NiO_x from the reduction of Ni^{3+} cations to Ni^{2+} during the Ar plasma cleaning step, typically used to improve the wettability of the oxide, thus maintaining NiO_x conductivity. The Ni_yN layer also passivates the interface between NiO_x and $MAPbI_3$ and inhibits the reaction between $MAPbI_3$ and Ni^{3+}. Although Ni_yN is conductive and could be expected to introduce trap states that damage PV performance, we show that thin enough Ni_yN can passivate the interface between NiO_x and HaP, thereby improving device efficiency and stability.

EXPERIMENTAL SECTION

Fabrication. *Substrate Cleaning.* Fluorine-doped tin oxide (FTO, KINTEC Company)-coated glass substrates (TEC 15, 1 inch × 1 inch) were cleaned in a sonication bath with soap (Decon 90) and deionized water and then rinsed in deionized water followed by dry ethanol.

NiO_x and Ni_yN were deposited using RF sputtering (AJA International Inc.) from 2-inch NiO and Ni targets, respectively (Kurt J. Lesker, 99.9%). NiO_x deposition was done at room temperature with an Ar gas flow of 30 sccm and a total chamber pressure of 3 mTorr. Ni_yN deposition was done at room temperature and a total chamber pressure of 3 mTorr, with Ar and N_2 gas flows of 15 and 45 sccm, respectively. In the first stage, the NiO_x target was set to 80 W for 1 h, then the chamber was purged for 10 min, and finally, the Ni target was set to 60 W for 3 min. Ar plasma cleaning was performed by applying a power of 30 W on the substrate with an Ar flow of 30 sccm.

$MAPbI_3$ was synthesized from MAI (Greatcell Solar) and PbI_2 (Sigma-Aldrich, 99.999%) precursors in a 1:1 ratio at a concentration of 1.5 M. The precursors were dissolved overnight at 60 °C in γ-butyrolactone (GBL, Alfa Aesar, 99%) and dimethyl sulfoxide (DMSO, Sigma-Aldrich, anhydrous) at a 7:3 ratio. The solution was spin-coated at 4000 rpm for 35 s with 800 μL of a toluene (Sigma-Aldrich, anhydrous) anti-solvent drip after 30 s. For device fabrication, 20 mg of PCBM was dissolved in 1 mL of chlorobenzene overnight, spin-coated at 2000 rpm for 30 s, and annealed for 10 min. After 15 min of cooling, a solution of 3 mg of bathocuproine in 6 mL of isopropanol was spin-coated at 4000 rpm for 30 s. Finally, thermal evaporation was performed to deposit round Ag contacts of 3 mm diameter. A scheme of the device structure is given in the Supporting Information (SI) (Figure S1).

Characterization. Ultraviolet photoemission spectroscopy (UPS) was used to probe the vacuum level and the position of the Fermi level with respect to the valence band edge, leading to the determination of the work function (WF) and ionization energy (IE) of the measured materials at a resolution of 0.15 eV. UPS was performed in an ultrahigh vacuum (10^{-10} Torr) with He I photons (21.22 eV) generated by a He discharge lamp, with a pass energy of 5 eV and a 0.02 eV step size.

X-ray photoelectron spectroscopy (XPS) with an Al Kα anode (1486.6 eV) was used to probe the Ni 2p, N 1s, and C 1s core levels at a resolution of 0.8 eV. Scans were taken with a pass energy of 25 eV and a 0.05 eV step size at a low base pressure of 10^{-9} Torr. UPS and XPS were conducted on the samples before and after a 5 s Ar^+ etching. The Ar^+ etching was performed using an Ar ion gun at a pressure of 5.5×10^{-5} Torr, a 1000 V acceleration voltage, and a 20 mA emission current. The current measured during the etching process was around 15 μA. All UPS, XPS, and Ar^+ etching steps were performed in the same vacuum chamber without sample exposure to ambient atmosphere.

XPS in Bar-Ilan University (BIU) was performed using a Thermo Scientific Nexsa spectrometer XPS system with an Al Kα anode (1486.6 eV) at a base pressure of ~7×10^{-8} Pa (~5×10^{-10} Torr). The binding energy (BE) was calibrated vs carbon (C 1s = 285 eV). Survey scans were collected with a pass energy of 200 eV and a 1.0 eV step size, followed by high-resolution scans with a pass energy of 50 eV and a step size of 0.1 eV. The samples were exposed for ~1 min to air during the sample transfer.

https://doi.org/10.1021/acsami.2c11701
ACS Appl. Mater. Interfaces 2022, 14, 47587−47594

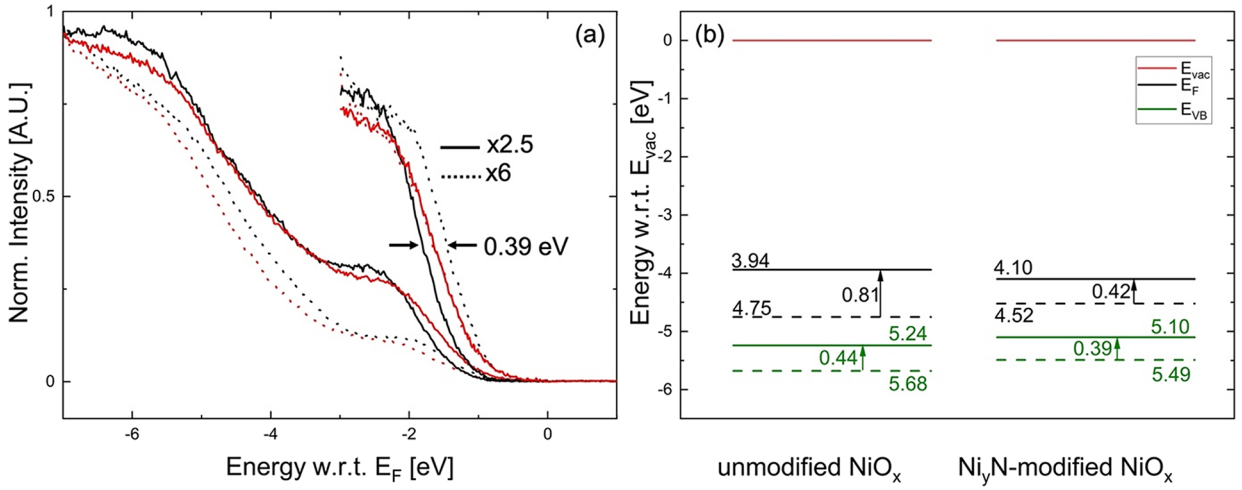

Figure 2. (a) Normalized UPS valence spectra plotted with respect to the Fermi level (E_F) for NiO_x (black) and Ni_yN-modified NiO_x (red) before (dashed) and after (solid) 5 s Ar^+ etching. (b) Energy diagrams for NiO_x (left) and Ni_yN-modified NiO_x (right) before (dashed) and after (solid) 5 s Ar^+ etching. All energy levels are plotted with respect to the vacuum level (E_{vac}). Energy diagrams plotted relative to the Fermi energy (E_f) are shown in the SI (Figure S4).

Optical transmission measurements were performed using an optical fiber-based custom-made system that consists of a CCD array spectrometer (USB4000, Ocean Optics) and two integrating spheres. The measurements were done over a 400−1000 nm spectral range with a circular diameter of 3 mm in a N_2 atmosphere.

Two-probe measurements were done with a Keithley 2400 source measurement unit (SMU) in a potential range of −0.5 to 0.5 V at a 50 mV/point rate.

J−*V* characteristics were measured with the same Keithley source at a potential range of −1.2 to 0.2 V at a 20 mV/point rate in ascending and descending scan directions. The device was illuminated through an optical fiber using a laser-driven light source (LDLS, EQ-99FC, Energetiq) xenon lamp calibrated to the AM1.5G solar spectrum.

Photoemission yield spectroscopy (PEYS) was used to measure the IE (valence band maximum energy, relative to the vacuum level) of perovskite surfaces. The measurements were done under a N_2 atmosphere, using an air photoemission system (ASKP150200, KP Technology Ltd.), illuminated by a deuterium (D_2) UV source, coupled with a motorized grating monochromator.

Transient PL decay measurements on the HaP thin films deposited on NiO/FTO substrates with and without a NiN interlayer were measured in ambient conditions. The HaP thin films were excited with a 450 nm picosecond pulsed laser diode source, and PL decay characteristics in the 760−765 nm emission wavelength range were recorded with a photomultiplier tube.

RESULTS AND DISCUSSION

We used RF sputtering to deposit a NiO_x layer from a NiO target on an FTO-coated glass substrate. To modify the NiO_x surface, we used reactive sputtering treatment of the Ni target with a plasma composition of 25% Ar and 75% N_2.

To examine the reactive sputtering effect on the NiO_x surface, we used XPS on NiO_x samples modified and unmodified by reactive sputtering. The XPS spectra from both NiO_x samples show a broad and shallow nitrogen signal around a binding energy of 399 eV, which typically fits the signal of nitrogen in organic matrices (Figure 1a).[26,27] However, the NiO_x layer after a reactive sputtering treatment of a Ni target with a plasma composition of 25% Ar and 75% N_2 exhibits a clear, sharp nitrogen peak at a binding energy of 397.7 eV that fits metal nitrides.

To examine the effect of the Ni_yN modification on NiO_x, we conducted 5 s of Ar^+ etching to clean the surface of contaminants and mimic the layers built into the solar cells. After Ar^+ etching, the intensity of C 1s is reduced, indicative of the surface cleaning effect of the 5 s etching process. The BE of the C 1s core level increases by 0.3 eV, from 284.9 to 285.2 eV, for both unmodified NiO_x and Ni_yN-modified NiO_x. Any carbon present in the layers is adventitious, and the BE difference is most likely due to a change in the chemical environment between the top and sub-surface species, as the surface is Ar^+ etched (Figure 1b).

Nickel and oxygen are not adventitious; hence, their BE can be more directly linked to the Fermi level (E_F) position in the material. The O 1s feature is a superposition of two core level peaks corresponding to oxygen bound to Ni^{3+} and Ni^{2+}. The BE of the O 1s peak is found to increase by 0.6 eV upon Ar^+ etching, from 528.6 to 529.2 eV, for NiO_x (Figure 1c) but only by 0.2 eV, from 528.7 to 528.9 eV, for Ni_yN-modified NiO_x (Figure 1e). O 1s peak fitting details can be found in Figure S2. Similarly, the BE of the tallest Ni 2p peak increases by 0.4 eV from 852.7 to 853.1 eV for NiO_x (Figure 1d) but remains unchanged at 853.2 eV for Ni_yN-modified NiO_x (Figure 1f).

To understand the effect of Ar^+ etching on the electronic structure of the NiO_x surface, we performed UPS to determine the WF and IE of the NiO_x films, both with and without Ni_yN modification. The valence band maximum (VBM) positions obtained by linear extrapolation of the leading edge of the filled states are shown in Figure 2a. Notably, the NiO_x valence band shows a 0.39 eV shift away from E_F upon Ar^+ etching, whereas the Ni_yN-modified NiO_x valence band remains at the same position (negligible shift of 0.03 eV). Comparing the valence bands of the NiO_x reference and Ni_yN-modified NiO_x after 5 s of Ar^+ etching, we find the VBM to be 0.30 eV closer to the Fermi level for Ni_yN-modified NiO_x (1.00 eV below E_F) than for the unmodified NiO_x (1.30 eV below E_F) (Figure 2). This trend is further investigated by measuring a 40 nm thick Ni_yN on NiO_x, whose VBM reaches all the way to the Fermi level, forming almost a Fermi step (Figure S3).

The resulting energy diagrams for NiO_x (left) and Ni_yN-modified NiO_x (right) before and after 5 s Ar^+ etching, plotted relative to the vacuum level (E_{vac}), are shown in Figure 2b. For clarity, similar energy diagrams, plotted relative to the Fermi energy (E_f), as they were measured, are shown in the SI

https://doi.org/10.1021/acsami.2c11701
ACS Appl. Mater. Interfaces 2022, 14, 47587−47594

(Figure S4). The WF for unmodified NiO_x decreases from 4.75 to 3.94 eV after 5 s Ar^+ etching and from 4.52 to 4.10 eV for Ni_yN-modified NiO_x. Together with the linearly extrapolated VBM values, the IE values are found to be 5.24 eV for Ar^+-etched, unmodified NiO_x and 5.10 eV for Ni_yN-modified NiO_x (Figure 2b). The UPS and XPS data suggest that the Ni_yN-modified NiO_x is more resistant to damage or to defects induced by the Ar^+ etching process than the unmodified NiO_x. The BEs of the Ni 2p and O 1s core levels remain comparable before and after Ar^+ etching for Ni_yN-modified NiO_x within the resolution of XPS, indicative of a nearly unchanged Fermi level position before and after the etching process. At the same time, the unmodified NiO_x layer shows an increase in BE for both Ni 2p and O 1s core levels, reflecting a Fermi level shift toward the middle of the NiO_x gap.

NiO_x is typically not fully stoichiometric. Based on the presence of Ni^{3+} (Figure S2) and the p-type character of the film, as shown by the position of the Fermi level in the lower part of the gap (Figure 2b), we infer that the NiO_x we synthesized is O-rich as reported in the literature.[10,28] The charge carrier (hole) density in the NiO_x is the result of nickel vacancies (V''_{Ni}) and/or oxygen interstitials (O''_i).[29] Ar^+ etching presumably creates more oxygen vacancies ($V^{\cdot\cdot}_O$), because oxygen is lighter than nickel and, thus, more easily ejected from the etched surface. Oxygen vacancies can reduce the charge carrier concentration as $V^{\cdot\cdot}_O + O''_i \rightarrow \frac{1}{2}O_2\uparrow$, and thereby reduce the p-doping level of the NiO_x films. Ni_yN-modified NiO_x is more resistant to such a process, as seen by the XPS and UPS results, demonstrating the passivating effects of Ni_yN on the NiO_x surface. This passivating effect makes the Ni_yN-modified NiO_x film less prone to electronic structure changes during subsequent processing steps, which is further corroborated by the unchanged energies of the valence states with respect to the Fermi level in Figure 2a.

As a minor point, the decrease in the adventitious C 1s peak intensity upon Ar^+ etching of both surfaces (Figure 1b) is consistent with a ~0.4 eV vacuum level (E_{vac}) shift, which agrees with the 0.42 eV change in the Ni_yN-modified NiO_x WF measured by UPS (a decrease in E_{vac} from 4.52 to 4.10 eV as seen in Figure S4) above E_F upon Ar^+ etching (Figure 2b). For unmodified NiO_x, however, the WF decreases by 0.8 eV, a combination of an ~0.4 eV decrease in E_{vac} and an ~0.4 eV downward shift of the band edges with respect to E_F. To check if the effect of Ar^+ etching performed in the XPS measurements resembles that of the Ar plasma cleaning, performed via RF sputtering, of the unmodified NiO_x and Ni_yN-modified NiO_x surfaces, we used 60 s RF sputtering with Ar plasma to etch NiO_x with and without Ni_yN modification, to imitate the conditions before $MAPbI_3$ spin coating.

The impact of the Ar plasma on the optical transparency of the unmodified NiO_x and the Ni_yN-modified NiO_x was examined via total transmission measurements over a range of 370−950 nm. We found that in the visible range, Ar plasma treatment did not change the transparency of the unmodified NiO_x. The Ni_yN modification reduced NiO_x transparency by ~1.5%, which is expected because of the narrow band gap of Ni_yN. The Ar plasma treatment etched away part of the Ni_yN and improved the transparency to bring it closer to that of the unmodified NiO_x (Figure 3a). The Ar plasma effect on the Ni_yN-modified NiO_x, together with the lack of change in the E_F position in the material's gap seen by XPS and UPS, suggests that the Ni_yN forms a protective layer on top of the

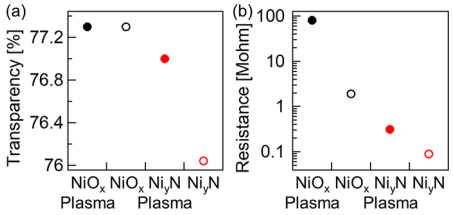

Figure 3. (a) UV−vis total optical transmission (TT) and (b) electrical resistance (logarithmic scale) measurement data of a reference NiO_x (black) and of a Ni_yN-modified NiO_x (red) sample that was not etched (open) and after Ar plasma etching for 60 s (solid). Each mark in both plots is the average of nine measured points with an error range of ±0.4% for the transparency and ±10% for the resistance measurements.

NiO_x, preventing a reaction between the NiO_x and the Ar plasma.

The NiO_x film protection by the Ni_yN layer from the Ar plasma was investigated via two-probe electrical measurements, inspecting the resistance along the Z axis (perpendicular to the surface) between the FTO electrode and the NiO_x surface with and without a Ni_yN layer, both before and after Ar plasma treatment. The Ar plasma treatment dramatically increased the unmodified NiO_x resistance ~40×, from 1.9 MΩ before to 80 MΩ after. The Ni_yN layer reduced the NiO_x resistance from 1.9 to 0.09 MΩ before plasma treatment, but even more critically, after Ar plasma treatment, the resistance increased about three times to 0.3 MΩ, lower than that of the unmodified NiO_x (Figure 3b). The dramatic resistance increase of the unmodified NiO_x after the Ar plasma treatment via RF sputtering indicates a decrease in O''_i concentration in the NiO_x film, which reduces the NiO_x surface. This interpretation fits the results from XPS, which shows that Ar^+ etching leads to a decrease in the Ni^{3+}/Ni^{2+} ratio. The likely cause is that RF Ar plasma sputtering, similar to Ar^+ etching, removes more of the lighter oxygen atoms than of the heavier Ni atoms, leading to $V^{\cdot\cdot}_O$ and reduction in the NiO_x p-doping levels. The result is that the NiO_x is less p-type and becomes less conductive. The Ni_yN layer modification decreases the resistance by around 20×, and while it increases after Ar plasma, the resistance is still six times smaller than that of NiO_x before Ar plasma treatment. The XPS measurements suggest an explanation for preserving the low resistance after Ar plasma by applying the Ni_yN layer, namely, that the original Ni^{3+} concentration is retained. The results from UPS are consistent with the resistance decrease after Ni_yN modification of NiO_x. The energy of the VBM is closer to E_F after Ni_yN modification; the IE, 5.1 eV, is smaller than that of the unmodified NiO_x, 5.24 eV, which improves the contact with a gold probe (WF ~5.1 eV). The VBM shift toward E_F as Ni_yN gets thicker may explain the minor resistance increase after Ar plasma, as part of the Ni_yN layer is etched away.

After measuring the transparency and resistance of NiO_x with and without Ni_yN, before and after plasma etching, we marked Ni_yN-modified NiO_x after plasma treatment as the best candidate for PSCs. Thus, we deposited $MAPbI_3$ on top of NiO_x with and without a Ni_yN layer after plasma treatment and then performed time-resolved photoluminescence (TRPL) to measure differences in charge extraction after Ni_yN deposition and plasma treatment. A fit of the PL decay to a double exponential curve typically indicates two kinds of decay mechanisms, which are common when HaP is deposited on a selective contact.[30−34] A short lifetime τ_1 corresponds to

https://doi.org/10.1021/acsami.2c11701
ACS Appl. Mater. Interfaces 2022, 14, 47587−47594

charge transfer and detrapping of charge due to light exposure, and a longer lifetime τ_2 corresponds to recombinations at the interface and within the absorber. Because τ_1 and τ_2 were hard to distinguish, we chose to calculate only τ_2 according to a monoexponential fit at a decay time > 60 ns.[35] Similar lifetimes, 31 and 29 ns for $MAPbI_3$ on NiO_x and Ni_yN-modified NiO_x, respectively (Figure 4a), indicate that Ni_yN modification did not cause more (or less) recombination at the interface. Furthermore, PEYS, AFM, SEM, and XRD measurements (Figure 4b and Figures S5−S7) do not differ between $MAPbI_3$ layers deposited on Ni_yN-modified or unmodified NiO_x.

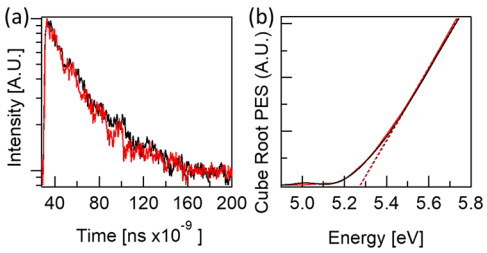

Figure 4. (a) TRPL and (b) PEYS measurements of $MAPbI_3$, deposited on plasma-etched Ni_yN-modified NiO_x (red) and unmodified NiO_x (black), both on an FTO substrate and after plasma etching.

AFM imaging of the surfaces before and after Ni_yN modification does not show any difference in morphology (Figure S5).

SEM and XRD (Figures S6 and S7) measurements show no significant difference in $MAPbI_3$ morphology and crystallinity (peak presence, positions, and widths). Both XRD analysis and SEM micrographs did not show any signs of PbI_2 beyond the peak-to-noise ratio level.

PEYS (Figure 4b) yielded the same values for the $MAPbI_3$ IE between samples deposited on NiO_x or Ni_yN-modified NiO_x in dry N_2.

The $MAPbI_3$ surface morphology similarities before and after Ni_yN modification of NiO_x and the PEYS and XRD results indicate and even imply that the solar cell efficiency improvement in these samples is caused by the Ni_yN layer effect on the NiO_x selective contact rather than an effect on the $MAPbI_3$ layer.

To test the photovoltaic activity of the Ni_yN-modified cells, $I-V$ measurements, in the dark and under illumination, were recorded on all complete PSCs in both ascending and descending voltage scan directions (Figure S8), but only the descending direction is shown for simplicity (Figure 5a). Statistics on 30 PSCs reveal that the Ni_yN passivation layer affects the entire device in two main ways. As the etching time is decreased, the Ni_yN layer becomes thicker, and the V_{oc} decreases from an average of 1.05 V for cells with unmodified NiO_x to 0.8 V for Ni_yN with no plasma etching (Figure 5b). V_{oc} highly depends on the Ni_yN thickness, and most of the 0.25 V V_{oc} loss is gained back as the Ar plasma treatment increases, and Ni_yN gets thinner, up to a negligible value of 0.01 V. This effect of the Ni_yN thickness on V_{oc} can be linked to the UPS-measured VBM shift of up to 0.37 eV toward E_F as the ∼2 nm Ni_yN thickness increases, all the way to the Fermi level when the Ni_yN is 40 nm thick (Figure S3). The similarity in V_{oc} between these two samples is consistent with the similar results obtained by TRPL. At the same time, the FF improves

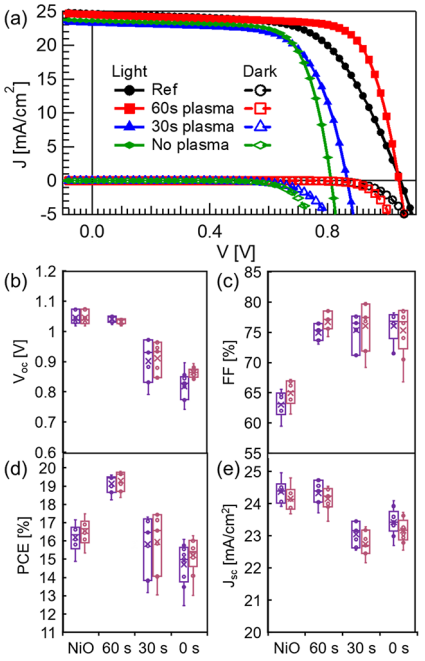

Figure 5. (a) $I-V$ curves in the dark (dashed) and under illumination (solid) of representative PSCs with NiO_x (black circles) and an additional Ni_yN layer after 60 s (red squares), 30 s (blue triangles), and no Ar plasma etching (green rhombohedrons). (b−e) Statistical distributions of the photovoltaic parameters for 30 PSCs employing as HTM NiO_x and NiO_x after depositing a Ni_yN layer onto it, after 60 s, 30 s, and no Ar plasma etching, in the descending (pink) and ascending (purple) scans: (b) V_{oc}, (c) FF, (d) PCE, and (e) J_{sc}.

dramatically from a 65% average with unmodified NiO_x to 75% with the Ni_yN layer, regardless of its thickness or the etching time (Figure 5c). The FF improvement for the Ni_yN-modified PSCs indicates that despite its metallic properties, the Ni_yN layer was thin enough so that no obvious damaging trap states formed at the interface with $MAPbI_3$.

The minor decrease in V_{oc} and the significant improvement in the FF yield an overall PCE improvement, from a 16.5% average and a 17.4% record cell for the reference NiO_x to a 19.2% average and a 19.8% record cell for NiO_x with a Ni_yN layer after 60 s of Ar plasma (Figure 5d). A slight decrease of 2 mA in J_{sc} for PSCs with a shorter Ni_yN etching time (Figure 5e) is consistent with a slightly lower external quantum efficiency (EQE) (Figure S9) for these samples and is explained by the decrease in transparency, as seen in Figure 3a. Therefore, the proposed optimum use of our Ni_yN modification is to have as thin a Ni_yN layer on NiO_x as possible, which can passivate the HTL with a minimum loss in V_{oc} and transparency.

To further investigate the huge effect that the Ni_yN layer has on the complete solar cell FF, we performed dark $I-V$ measurements to determine the shunt resistance (R_{sh}) and the series resistance (R_s) of the SC (Figure 6a,b, respectively). R_{sh} increased with the Ni_yN layer thickness, presumably due to the added coverage by the amorphous Ni_yN layer, which inhibited electrical shorts between the layers. R_s dramatically dropped whenever Ni_yN was deposited and decreased further with thicker Ni_yN layers but with a minor trend. After summing up our former observations of UPS, XPS, transparency, and resistance, we conclude that the significant R_s decrease after Ni_yN deposition is due to a higher Ni^{3+} concentration within

https://doi.org/10.1021/acsami.2c11701
ACS Appl. Mater. Interfaces 2022, 14, 47587−47594

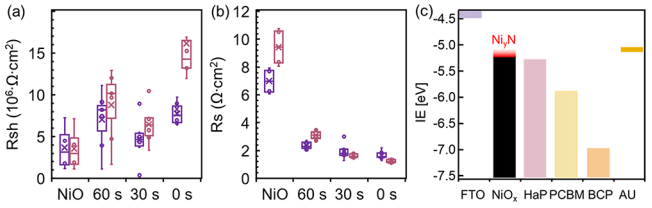

Figure 6. (a) Shunt resistance and (b) series resistance as measured from dark $I-V$ measurements. (c) IE values (i.e., VBM), measured from the vacuum level, of the layers composing the SC stacks.

NiO_x, when the Ni_yN layer is present. The minor trend of R_s decrease is inversely related to the Ar plasma etching time and follows the thickness of the Ni_yN layer. Based on the interpretation of the UPS measurement (Figure 2a and Figure S3), we ascribe this to a VBM shift toward the vacuum level that increases the driving force for hole extraction from the HaP film but at the expense of the V_{oc} (Figure 6c).

To test the effect of the Ni_yN modification on cell stability, 18 cells were measured over 4 days at room temperature in a N_2-filled chamber with a controlled environment and relative humidity that did not surpass 5%. The cells were held in the dark between the measurements and were exposed to light for 4 h before and naturally during measurements. For both types of cells, the PCE decreased over the 4 days. However, on average, the reference cell PCE values were reduced by almost 50%, from 15.9 to 9%, while those of the Ni_yN-modified cells were reduced only by 15%, from 16.5 to 14% (Figure 7a).

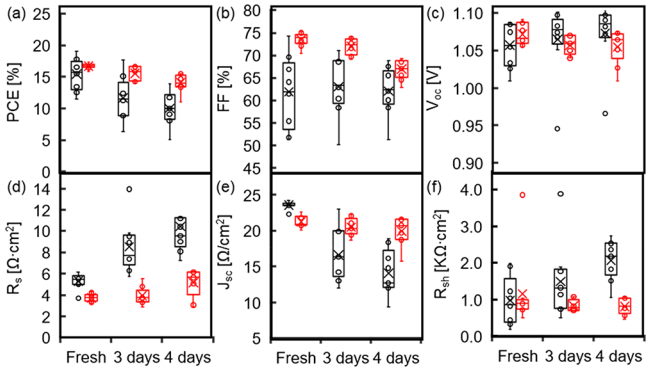

Figure 7. Statistical photovoltaic parameters of 18 PSCs over 4 days, employing NiO_x as an HTL with Ni_yN (red) and without (black) modification. Measurements were done in a descending scan direction: (a) PCE, (b) FF, (c) V_{oc}, (d) R_s, (e) J_{sc}, and (g) R_{sh}.

Further investigation of the SC statistics reveals a different aging mechanism for cells with Ni_yN than those without it. The V_{oc} and J_{sc} of both types of cells show inverse changes over the 4 days of testing. The J_{sc} of the reference cells decreased by 40% to, on average, 14 mA/cm^2, whereas the J_{sc} of the Ni_yN-modified cells remained almost constant at 20 mA/cm^2 (Figure 7e). The V_{oc} of the reference cells increased by 3% up to 1.1 V, and the V_{oc} of the Ni_yN-modified cells decreased by 8% down to 0.95 V (Figure 7c). The FF values remained the same (63% without and 73% with Ni_yN modified-NiO_x; see Figure 7b). The series and shunt resistances of the reference cells increased gradually over 4 days by more than 90%. However, the series and the shunt resistances of the Ni_yN-modified cells remained constant for 3 days, and only on the fourth day did the series resistance increase by 30% (Figure 7d,f), still a much lower factor than that of the reference cells. The rapid J_{sc} reduction and the R_s increase in untreated PSCs are prominent evidence of a reaction at the NiO_x–$MAPbI_3$ interface inhibited by the Ni_yN treatment. The Ni_yN layer plays a dual role, as it helps maintain the Ni^{3+} concentration, passivates the NiO_x–$MAPbI_3$ interface, and presumably prevents a reaction between the more active Ni^{3+} and $MAPbI_3$. These two features of the Ni_yN layer improve the solar device FF and, most importantly, cell stability.

To further investigate the current reduction source, we measured $I-V$ characteristics over 4 days, but this time we repeated the $I-V$ measurements for 100 cycles every day (Figure 8a,b). The reference cells exhibit an obvious current

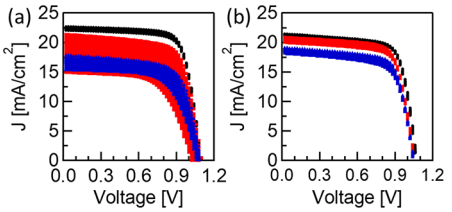

Figure 8. $I-V$ curves of fresh (black), 3-day-old (red), and 4-day-old (blue) cells with (a) a NiO_x HTL and (b) a Ni_yN-modified HTL.

reduction when the number of cycles increases, while the Ni_yN-modified cells do not. Although in the initial response, the shunt resistance of the reference cell is higher than that of the Ni_yN-modified SC, its series resistance is higher by 150%, which leads to the two types of cells having equal FFs. After 4 days of cycling, the series resistance of the reference cell increased by 70%. Similar to what Khenkin et al.[36] showed, the initial V_{oc} of the reference PSC started every day at 1.1 V but decreased as the number of cycles progressed, which is not the case for the Ni_yN-modified cells. We interpret this finding as an acceleration of the reaction at the interface by the constant change in the electric field applied to the SC under working conditions. The J_{sc} and R_s reductions suggest that an insulating interfacial layer formed between NiO_x and $MAPbI_3$. In contrast, in the cells prepared with Ni_yN-treated NiO_x, J_{sc} only undergoes a 3 mA/cm^2 loss over the 100 cycles. The constant R_s and R_{sh} over time indicate no change in charge transport and therefore no change of the material under working conditions. These results altogether support that Ni_yN modification inhibits reaction at the NiO_x–$MAPbI_3$ interface and prevents the formation of a blocking layer that deteriorates the SC performance.

CONCLUSIONS

We used a physical vapor deposition method to improve NiO_x HTLs with Ni_yN inorganic layers, which is the first time that such a modification was ever done. We showed that Ni_yN plays a dual role, improving the PSC's efficiency and stabilizing the NiO_x–HaP interface. The Ni_yN layer formed on NiO_x retains the Ni^{3+} species within the nickel oxide bulk, preserving its conductivity and thereby improving the overall cell efficiency. Furthermore, the same Ni_yN layer protects HaP from the reactive Ni^{3+} species, necessary for nickel oxide conductivity, and prevents degradation of HaP, giving devices superior stability over those built with untreated reference NiO films. Although, with time, some of the Ni_yN might be oxidized by the NiO_x layer, in a well-encapsulated device, the interfacial reactivity can be kept below the level where charged defects

https://doi.org/10.1021/acsami.2c11701
ACS Appl. Mater. Interfaces 2022, 14, 47587–47594

will start to change the overall defect density of the transport and absorber layers. These interactions should be investigated further beyond the scope of this study. We also showed that when Ni_yN is thin enough, its small energy gap, which can block sunlight and introduce traps for charge carriers at the interface, has a negligible effect on the overall SC efficiency. Our first reported solid-state, inorganic, in situ passivation route via RF sputtering deposition presents a major step toward solvent-free fabrication of reproducible and stable PSCs.

■ ASSOCIATED CONTENT

Supporting Information

The Supporting Information is available free of charge at https://pubs.acs.org/doi/10.1021/acsami.2c11701.

Scheme of the cell structure, XPS peak fitting of the O 1s peak, UPS and IPES measurements of ∼40 nm Ni_yN, energy diagrams for the NiO_x and Ni_yN-modified NiO_x vs E_F, AFM scans, SEM micrographs of $MAPbI_3$, XRD plot for $MAPbI_3$, $I-V$ curves in ascending and descending directions, and EQE of PSCs with different Ni_yN etching times (PDF)

■ AUTHOR INFORMATION

Corresponding Authors

Antoine Kahn − *Department of Electrical and Computer Engineering, Princeton University, Princeton, New Jersey 08544, United States;* orcid.org/0000-0002-1612-3350; Email: kahn@princeton.edu

David Cahen − *Department of Chemistry and Bar-Ilan Institute for Nanotechnology & Advanced Materials, Bar-Ilan University, Ramat Gan 5290002, Israel; Weizmann Institute of Science, Rehovot 7610001, Israel;* orcid.org/0000-0001-8118-5446; Email: david.cahen@weizmann.ac.il

Authors

Anat Itzhak − *Department of Chemistry and Bar-Ilan Institute for Nanotechnology & Advanced Materials, Bar-Ilan University, Ramat Gan 5290002, Israel;* orcid.org/0000-0002-1764-692X

Xu He − *Department of Electrical and Computer Engineering, Princeton University, Princeton, New Jersey 08544, United States;* orcid.org/0000-0002-0215-4666

Adi Kama − *Department of Chemistry and Bar-Ilan Institute for Nanotechnology & Advanced Materials, Bar-Ilan University, Ramat Gan 5290002, Israel;* orcid.org/0000-0001-5185-8873

Sujit Kumar − *Department of Chemistry and Bar-Ilan Institute for Nanotechnology & Advanced Materials, Bar-Ilan University, Ramat Gan 5290002, Israel; Weizmann Institute of Science, Rehovot 7610001, Israel;* orcid.org/0000-0003-0294-7575

Michal Ejgenberg − *Department of Chemistry and Bar-Ilan Institute for Nanotechnology & Advanced Materials, Bar-Ilan University, Ramat Gan 5290002, Israel*

Complete contact information is available at: https://pubs.acs.org/10.1021/acsami.2c11701

Author Contributions

‖A.I. and X.H. contributed equally.

Author Contributions

D.C. and A.I. conceptualized the project. D.C. and A. Kahn supervised the project. A.I. synthesized and fabricated the layers and the solar cells and investigated and carried out the electrical measurements, XRD, and SEM characterization. X.H. investigated and carried out most of the XPS, IPES, and UPS characterization. A. Kama helped with RF sputtering depositions and helped with the draft writing. S.K. carried out TRPL measurements and helped with the draft writing. M.E. carried out some of the XPS measurements. The manuscript was written through the contributions of all authors. All authors have approved the final version of the manuscript.

Notes

The authors declare no competing financial interest.

■ ACKNOWLEDGMENTS

The authors thank Dr. Eti Teblum (BIU) for AFM measurements, Shay Tirosh for his help with the EQE measurements, and Ziv Ben Daniel for insightful discussions. A.I. thanks the Israel Ministry of Science & Technology for the PhD fellowship support. This research was supported by Grant No. 2018349 from the United States-Israel Binational Science Foundation (BSF). S.K. held an Israel Council of Higher Learning PBC/VATAT PD fellowship at Bar-Ilan University. At the Weizmann Institute of Science, the work was supported by the WIS Sustainability and Energy Research Initiative (SAERI).

■ REFERENCES

(1) Kim, G. W.; Petrozza, A. Defect Tolerance and Intolerance in Metal-Halide Perovskites. *Adv. Energy Mater.* **2020**, *10*, 2001959.

(2) Rakita, Y.; Lubomirsky, I.; Cahen, D. When Defects Become 'Dynamic': Halide Perovskites: A New Window on Materials? *Mater. Horiz.* **2019**, *6*, 1297.

(3) Cohen, A. V.; Egger, D. A.; Rappe, A. M.; Kronik, L. Breakdown of the Static Picture of Defect Energetics in Halide Perovskites: The Case of the Br Vacancy in CsPbBr3. *J. Phys. Chem. Lett.* **2019**, *10*, 4490−4498.

(4) Schulz, P.; Cahen, D.; Kahn, A. Halide Perovskites: Is It All about the Interfaces? *Chem. Rev.* **2019**, *119*, 3349−3417.

(5) Lira-Cantú, M. Perovskite Solar Cells: Stability Lies at Interfaces. *Nat. Energy* **2017**, *2*, 17115.

(6) Jeng, J. Y.; Chen, K. C.; Chiang, T. Y.; Lin, P. Y.; Tsai, T. D.; Chang, Y. C.; Guo, T. F.; Chen, P.; Wen, T. C.; Hsu, Y. J. Nickel Oxide Electrode Interlayer in CH3NH3PbI 3 Perovskite/PCBM Planar-Heterojunction Hybrid Solar Cells. *Adv. Mater.* **2014**, *26*, 4107−4113.

(7) Tian, H.; Xu, B.; Chen, H.; Johansson, E. M. J.; Boschloo, G. Solid-State Perovskite-Sensitized p-Type Mesoporous Nickel Oxide Solar Cells. *ChemSusChem* **2014**, *7*, 2150−2153.

(8) Islam, M. B.; Yanagida, M.; Shirai, Y.; Nabetani, Y.; Miyano, K. Highly Stable Semi-Transparent MAPbI 3 Perovskite Solar Cells with Operational Output for 4000 h. *Sol. Energy Mater. Sol. Cells* **2019**, *195*, 323−329.

(9) Kim, H. S.; Seo, J. Y.; Park, N. G. Impact of Selective Contacts on Long-Term Stability of CH3NH3PbI3 Perovskite Solar Cells. *J. Phys. Chem. C* **2016**, *120*, 27840−27848.

(10) Wang, K.-C.; Shen, P.-S.; Li, M.-H.; Chen, S.; Lin, M.-W.; Chen, P.; Guo, T.-F. Low-Temperature Sputtered Nickel Oxide Compact Thin Film As. *ACS Appl. Mater. Interfaces* **2014**, *6*, 11851−11858.

(11) Islam, M. B.; Yanagida, M.; Shirai, Y.; Nabetani, Y.; Miyano, K. NiOx Hole Transport Layer for Perovskite Solar Cells with Improved Stability and Reproducibility. *ACS Omega* **2017**, *2*, 2291−2299.

(12) Cai, L.; Zhu, F. Toward Efficient and Stable Operation of Perovskite Solar Cells: Impact of Sputtered Metal Oxide Interlayers. *Nano Sel.* **2021**, *2*, 1417−1436.
(13) Alghamdi, A. R. M.; Yanagida, M.; Shirai, Y.; Andersson, G. G.; Miyano, K. Surface Passivation of Sputtered NiOxUsing a SAM Interface Layer to Enhance the Performance of Perovskite Solar Cells. *ACS Omega* **2022**, *7*, 12147−12157.
(14) Boyd, C. C.; Shallcross, R. C.; Moot, T.; Kerner, R.; Bertoluzzi, L.; Onno, A.; Kavadiya, S.; Chosy, C.; Wolf, E. J.; Werner, J.; Raiford, J. A.; de Paula, C.; Palmstrom, A. F.; Yu, Z. J.; Berry, J. J.; Bent, S. F.; Holman, Z. C.; Luther, J. M.; Ratcliff, E. L.; Armstrong, N. R.; McGehee, M. D. Overcoming Redox Reactions at Perovskite-Nickel Oxide Interfaces to Boost Voltages in Perovskite Solar Cells. *Joule* **2020**, *4*, 1759−1775.
(15) Zhao, Q.; Fang, C.; Tie, F.; Luo, W.; Peng, Y.; Huang, F.; Ku, Z.; Cheng, Y. B. Regulating the Ni3+/Ni2+ Ratio of NiOx by Plasma Treatment for Fully Vacuum-Deposited Perovskite Solar Cells. *Mater. Sci. Semicond. Process.* **2022**, *148*, 106839.
(16) Traore, B.; Pedesseau, L.; Blancon, J. C.; Tretiak, S.; Mohite, A. D.; Even, J.; Katan, C.; Kepenekian, M. Importance of Vacancies and Doping in the Hole-Transporting Nickel Oxide Interface with Halide Perovskites. *ACS Appl. Mater. Interfaces* **2020**, *12*, 6633−6640.
(17) Thakur, U. K.; Kumar, P.; Gusarov, S.; Kobryn, A. E.; Riddell, S.; Goswami, A.; Alam, K. M.; Savela, S.; Kar, P.; Thundat, T.; Meldrum, A.; Shankar, K. Consistently High Voc Values in P-i-n Type Perovskite Solar Cells Using Ni3+-Doped NiO Nanomesh as the Hole Transporting Layer. *ACS Appl. Mater. Interfaces* **2020**, *12*, 11467−11478.
(18) Pant, N.; Kulkarni, A.; Yanagida, M.; Shirai, Y.; Miyasaka, T.; Miyano, K. Residual PbI2 Beneficial in the Bulk or at the Interface? An Investigation Study in Sputtered NiO XHole-Transport-Layer-Based Perovskite Solar Cells. *ACS Appl. Energy Mater.* **2020**, *3*, 6215−6221.
(19) Pant, N.; Yanagida, M.; Shirai, Y.; Miyano, K. Effect of Different Surface Treatments of Sputtered NiO X on the Photovoltaic Parameters of Perovskite Solar Cells: A Correlation Study. *Appl. Phys. Express* **2020**, *13*, 025505.
(20) Pant, N.; Kulkarni, A.; Yanagida, M.; Shirai, Y.; Yashiro, S.; Sumiya, M.; Miyasaka, T.; Miyano, K. Passivation of Bulk and Interface Defects in Sputtered-NiOx-Based Planar Perovskite Solar Cells: A Facile Interfacial Engineering Strategy with Alkali Metal Halide Salts. *ACS Appl. Energy Mater.* **2021**, *4*, 4530.
(21) Di Girolamo, D.; Phung, N.; Jošt, M.; Al-Ashouri, A.; Chistiakova, G.; Li, J.; Márquez, J. A.; Unold, T.; Korte, L.; Albrecht, S.; Di Carlo, A.; Dini, D.; Abate, A. From Bulk to Surface: Sodium Treatment Reduces Recombination at the Nickel Oxide/Perovskite Interface. *Adv. Mater. Interfaces* **2019**, *6*, 1900789.
(22) Wu, F.; Pathak, R.; Chen, C.; Tong, Y.; Xu, H.; Zhang, T.; Jian, R.; Li, X.; Qiao, Q. Reduced Hysteresis in Perovskite Solar Cells Using Metal Oxide/Organic Hybrid Hole Transport Layer with Generated Interfacial Dipoles. *Electrochim. Acta* **2020**, *354*, 136660.
(23) Bai, S.; Da, P.; Li, C.; Wang, Z.; Yuan, Z.; Fu, F.; Kawecki, M.; Liu, X.; Sakai, N.; Wang, J. T. W.; Huettner, S.; Buecheler, S.; Fahlman, M.; Gao, F.; Snaith, H. J. Planar Perovskite Solar Cells with Long-Term Stability Using Ionic Liquid Additives. *Nature* **2019**, *571*, 245−250.
(24) Pérez-Del-Rey, D.; Boix, P. P.; Sessolo, M.; Hadipour, A.; Bolink, H. J. Interfacial Modification for High-Efficiency Vapor-Phase-Deposited Perovskite Solar Cells Based on a Metal Oxide Buffer Layer. *J. Phys. Chem. Lett.* **2018**, *9*, 1041−1046.
(25) Ávila, J.; Momblona, C.; Boix, P. P.; Sessolo, M.; Bolink, H. J. Vapor-Deposited Perovskites: The Route to High-Performance Solar Cell Production? *Joule* **2017**, *1*, 431−442.
(26) Naumkin, A. V.; Kraut-Vass, Anna Gaarenstroom, S. W.; Powell, C. J.*NIST X-ray Photoelectron Spectroscopy Database, Version 4.1*. https://srdata.nist.gov/xps/.
(27) Moulder, J. F.; Stickle, W. F.; Sobol, P. E.; Bomben, K. D.*Handbook of X-ray Photoelectron Spectroscopy*; Chastain, J., Ed.; Perkin-Elmer Corporation, Physical Electronics Division, 1992.
(28) Christian, J. D.; Gilbreath, W. P. Defect Structure of NiO and Rates and Mechanisms of Formation from Atomic Oxygen and Nickel. *Oxid. Met.* **1975**, *9*, 1−25.
(29) Mrowec, S.; Grzesik, Z. Oxidation of Nickel and Transport Properties of Nickel Oxide. *J. Phys. Chem. Solids* **2004**, *65*, 1651−1657.
(30) Kegelmann, L.; Wolff, C. M.; Awino, C.; Lang, F.; Unger, E. L.; Korte, L.; Dittrich, T.; Neher, D.; Rech, B.; Albrecht, S. It Takes Two to Tango - Double-Layer Selective Contacts in Perovskite Solar Cells for Improved Device Performance and Reduced Hysteresis. *ACS Appl. Mater. Interfaces* **2017**, *9*, 17245−17255.
(31) Stolterfoht, M.; Wolff, C. M.; Márquez, J. A.; Zhang, S.; Hages, C. J.; Rothhardt, D.; Albrecht, S.; Burn, P. L.; Meredith, P.; Unold, T.; Neher, D. Visualization and Suppression of Interfacial Recombination for High-Efficiency Large-Area Pin Perovskite Solar Cells. *Nat. Energy* **2018**, *3*, 847−854.
(32) Stolterfoht, M.; Caprioglio, P.; Wolff, C. M.; Márquez, J. A.; Nordmann, J.; Zhang, S.; Rothhardt, D.; Hörmann, U.; Amir, Y.; Redinger, A.; Kegelmann, L.; Zu, F.; Albrecht, S.; Koch, N.; Kirchartz, T.; Saliba, M.; Unold, T.; Neher, D. The Impact of Energy Alignment and Interfacial Recombination on the Internal and External Open-Circuit Voltage of Perovskite Solar Cells. *Energy Environ. Sci.* **2019**, *12*, 2778−2788.
(33) Kirchartz, T. High Open-Circuit Voltages in Lead-Halide Perovskite Solar Cells - Experiment, Theory and Open Questions. *Philos. Trans. R. Soc., A* **2019**, 20180286.
(34) Krogmeier, B.; Staub, F.; Grabowski, D.; Rau, U.; Kirchartz, T. Quantitative Analysis of the Transient Photoluminescence of CH 3 NH 3 PbI 3 /PC 61 BM Heterojunctions by Numerical Simulations. *Sustainable Energy Fuels* **2018**, *2*, 1027−1034.
(35) Kirchartz, T.; Márquez, J. A.; Stolterfoht, M.; Unold, T. Photoluminescence-Based Characterization of Halide Perovskites for Photovoltaics. *Adv. Energy Mater.* **2020**, *10*, 1904134.
(36) Khenkin, M. V.; Anoop, K. M.; Visoly-Fisher, I.; Kolusheva, S.; Galagan, Y.; Di Giacomo, F.; Vukovic, O.; Patil, B. R.; Sherafatipour, G.; Turkovic, V.; Rubahn, H. G.; Madsen, M.; Mazanik, A. V.; Katz, E. A. Dynamics of Photoinduced Degradation of Perovskite Photovoltaics: From Reversible to Irreversible Processes. *ACS Appl. Energy Mater.* **2018**, *1*, 799−806.

https://doi.org/10.1021/acsami.2c11701
ACS Appl. Mater. Interfaces 2022, 14, 47587−47594